# Generation of nearly nondiffracting Bessel beams with a Fabry–Perot interferometer

**Z. L. Horváth, M. Erdélyi, G. Szabó, and Zs. Bor**

*Department of Optics and Quantum Electronics, JATE University H-6720 Szeged, Dóm tér 9, Hungary*

**F. K. Tittel and J. R. Cavallaro**

*Rice University, Electrical & Computer Engineering Department, MS 366 6100 Main, Houston, Texas 77005-1892*

Received October 29, 1996; revised manuscript received April 8, 1997; accepted May 15, 1997

A new concept for generating zero-order Bessel beams was studied theoretically. The spatial intensity distribution was calculated numerically using a wave optics model. Approximate analytical expressions were derived to describe the radial intensity distribution in planes perpendicular to the optical axis of an imaging lens. © 1997 Optical Society of America [S0740-3232(97)00311-6]

## 1. INTRODUCTION

An ideal zero-order Bessel beam consists of a superposition of monochromatic plane waves with wave vectors lying on a conical surface having the same magnitude. Several experiments have been reported that achieve such a superposition of plane waves. For example, this type of angular spectrum can be obtained by applying an annular slit in the focal plane of a lens[1] or by the use of an axicon,[2] a holographic process,[3,4] a Fabry–Perot interferometer,[5,6] or a special type of laser cavity.[7,8]

A novel concept for the generation of nearly nondiffracting Bessel beams as applied to microlithography was described in Ref. 9. The experimental arrangement is shown in Fig. 1. A pointlike source was formed by focusing a He–Ne laser beam ($\lambda = 632.8$ nm). Such a point source illuminated a scanning Fabry–Perot interferometer, which produced a concentric ring system in front of a lens. The image produced by the lens was magnified by two microscope objectives, and the intensity distribution was observed with a CCD camera. The lens aperture was adjusted so that it transmitted only the first Fabry–Perot ring and blocked all other rings.

The measured intensity distribution in planes perpendicular to the optical axis is given by the $J_0$ function. This result was expected because a century ago[10–12] it was recognized that the diffraction pattern of a narrow annular aperture can be described by the zero-order Bessel function. Because of the annular illumination of the lens, the depth of focus increased and the transverse resolution could be improved by a factor of 1.6. This paper reports on an analytical wave optics description of experimental results obtained in Ref. 9.

## 2. THEORY

Figure 2 depicts a monochromatic spherical wave generated by a point source that illuminates a Fabry–Perot interferometer; the light passing through the interferometer is incident on a thin lens with focal length $f$ at wavelength $\lambda$. Because of multiple reflections in the interferometer, the electric field in front of the lens is the same as the field generated by a sequence of point sources $I_0, I_1, \ldots, I_m, \ldots$. The separation between two adjacent sources is $2d$ and their intensity ratio is $R^2$, where $d$ is the separation of the etalon of mirrors and $R$ is the reflectivity of the mirrors. The lens transforms the incoming spherical wave front generated by the $m$th source into a spherical wave front. The radius ($q_m$) of the wave front immediately after the exit surface of the lens is given by

$$1/q_m = 1/f - 1/p_m, \tag{1}$$

where $p_m$ is the radius of the incoming spherical wave front at the entrance surface of the lens. The lens aperture truncates the outgoing spherical wave so that the wave front is a spherical calotte (a segment of a spherical surface). The electric field produced by the $m$th source beyond the lens at point P can be obtained by calculating the diffraction integral[13] over the spherical calotte $SC$ (see Fig. 2):

$$\begin{aligned} E_m(r, z) &= -\frac{i}{\lambda}\frac{A_m \exp[ik(p_m + nD)]}{p_m}\iint_{SC}\frac{\exp(iks)}{s}\,\mathrm{d}S \\ &= \frac{q_m \exp[ik(p_m + nD + q_m)]}{p_m} \\ &\quad\times\left[-\frac{i}{\lambda}\frac{A_m \exp(-ikq_m)}{q_m}\iint_{SC}\frac{\exp(iks)}{s}\,\mathrm{d}S\right], \end{aligned} \tag{2}$$

where $r$ and $z$ are the cylindrical coordinates of point P, $A_m/p_m$ is the amplitude, and $kp_m$ is the phase of the incoming wave generated by the $m$th source, $k$ is the wave number, and $knD$ is the phase shift caused by the lens ($n$ is the refractive index, and $D$ is the axial thickness). The integral between the brackets has already been calculated in Ref. 13, and it leads to the well-known three-dimensional Airy pattern,

 © 1997 Optical Society of America

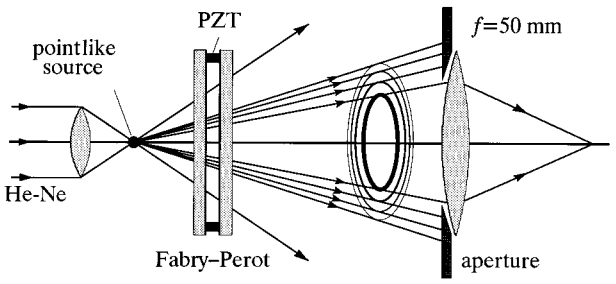


Fig. 1. Schematic diagram of the experimental setup for generating zero-order Bessel beams. A pointlike source illuminates a Fabry–Perot interferometer, which produces a concentric ring system in front of an imaging lens. If the aperture is adjusted so that it transmits the first Fabry–Perot ring only and blocks all others, a zero-order Bessel beam is generated beyond the lens.

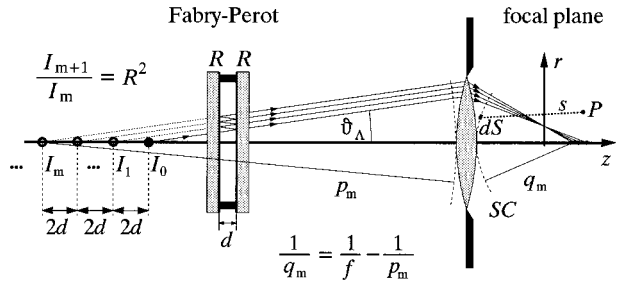


Fig. 2. Notation used for the calculations. Because of multiple reflections, the electric field in front of the lens is the same as the field generated by a sequence of point sources $I_0, I_1, \ldots, I_m, \ldots$. Beyond the lens the electric field is the superposition of the field produced by virtual point sources.

$$-\frac{i}{\lambda}\frac{A_m \exp(-ikq_m)}{q_m}\iint_{SC}\frac{\exp(iks)}{s}\,dS = -\frac{ikA_m a^2}{2q_m{}^2}\exp[i(q_m/a)^2 u_m] \times [C(u_m, v_m) - iS(u_m, v_m)], \quad (3)$$

where $a$ is the radius of the lens aperture, $C$ and $S$ functions can be calculated by the Lommel functions,[13] and $u_m$ and $v_m$ are dimensionless variables given by

$$u_m = k(a/q_m)^2(f + z - q_m),$$
$$v_m = k(a/q_m)r. \quad (4)$$

Inserting Eq. (3) and Eq. (4) into Eq. (2), we obtain

$$E_m(r, z) = -\frac{ikA_m{}^{a^2}\exp[ik(p_m + nD + f + z)]}{2p_m q_m} \times [C(u_m, v_m) - iS(u_m, v_m)]. \quad (5)$$

Since $A_m = R^m A_0$ and $p_m = p_0 + m2d$, Eq. (5) may be written as

$$E_m(r, z) = -\frac{ikR^m A_0{}^{a^2}\exp[ik(p_0 + nD + f + z + m2d)]}{2p_m q_m} \times [C(u_m, v_m) - iS(u_m, v_m)]. \quad (6)$$

The total electric field behind the lens is the sum of the fields of the individual sources,

$$E(r, z) = -\frac{ikA_0{}^{a^2}}{2}\exp[i(kz + \Phi_0)] \times \sum_{m=0}^{\infty}\frac{[R\exp(i\delta)]^m}{p_m q_m} \times [C(u_m, v_m) - iS(u_m, v_m)], \quad (7)$$

where $\Phi_0 = k(p_0 + nD + f)$ is an unimportant phase factor and

$$\delta = k2d = 4\pi d/\lambda \quad (8)$$

is the phase shift introduced by the Fabry–Perot interferometer. In the derivation of Eq. (7), we assumed that the phase change due to internal reflection in the etalon was zero. This effect can be taken into account by substituting $R\exp(i2\psi)$ for the reflectivity $R$ or increasing the etalon separation with a distance of $\psi/(2\pi)\lambda$, where $\psi$ is the phase change on internal reflection.

Eq. (8) yields the phase difference between two adjacent virtual sources. If $\Lambda$ denotes the largest integral value that is less than or equal to $2d/\lambda$, then one can define the reduced phase shift $\delta_r$ as

$$\delta_r = \frac{4(d - d_0)}{\lambda}\pi = K\pi, \quad (9)$$

where $d_0 = \Lambda\lambda/2$ and $K$ is a newly introduced parameter given by $4(d - d_0)/\lambda$. Thus $K$ varies from 0 to 2. A variation of $d$ of $\lambda/2$ leads to a change of $2\pi$ in the phase difference. For such a small variation of $d$, the position of image points of the virtual sources remains practically unchanged. Therefore $\delta_r$ and $d$ can be regarded as independent variables. This fact is important from the experimental point of view because it is difficult to measure the etalon separation with an accuracy of $\lambda$.

## 3. RESULTS AND DISCUSSION

If the lens is illuminated by a point source, the depth of focus of the image (DOF) is given by

$$\mathrm{DOF} = \frac{2\lambda}{NA^2}(1 + M)^2 \quad (10)$$

and is defined as the distance between the principal intensity maximum and the first intensity minimum on the optical axis, where $NA = a/f$ is the numerical aperture of the lens and $M$ is the magnification. The distance between the image points of the virtual sources approximately equals $2dM^2$. The relative image density defined by

$$N = \frac{\mathrm{DOF}}{2dM^2} = \frac{\lambda}{d}\left(\frac{1 + M}{NAM}\right)^2 \quad (11)$$

is an important quantity for determining the shape of the axial intensity distribution.[9]

In the previously reported experiment,[9] four different cases were studied. The focal length and the numerical aperture of the lens used in the experiment were 50 mm and 0.08929, respectively. The measured value of DOF

was 220 $\mu$m. For comparison these parameters are used. In this case from Eq. (10), the magnification is $M = 0.1772$ and the distance of source point $I_0$ from the lens is given by $p_0 = f + f/M = 332.17$ mm.

Figure 3 shows the intensity distribution for various values of image density $N$. The axial intensity distributions were fitted to the measured curves. The calculations were done by using Eq. (7) with the following parameters: (a) $d = 7431.6$ $\mu$m ($N = 0.47$), $K = 1.501$; (b) $d = 3100$ $\mu$m ($N = 1.13$), $K = 0.35$; (c) $d = 1091$ $\mu$m ($N = 3.21$), $K = 0.22$; (d) $d = 436.6$ $\mu$m ($N = 8.02$), $K = 0.164$. The reflectivity $R$ was assumed to be 0.963. These values of the parameters agree with their measured values within the accuracy of the measurement. The insets show the comparison of the measured (dots) and calculated (solid curves) intensity distribution on the optical axis.

In case (a) the distance between the image points on the optical axis is large compared with the DOF. Thus separate sharp peaks are clearly evident. By increasing the image density (i.e., decreasing $d$), we can make the oscillations on the optical axis disappear and the intensity curves become smoother. The numbers adjacent to the peaks show the value of the peak intensity. In agreement with the law of conservation of energy, the peak intensity increases with increasing $N$.

For certain circumstances the intensity distribution in a plane perpendicular to the optical axis can be described by a zero-order Bessel function. The radius of the interference rings is different for different cases and slightly increases with increasing $z$, as shown in Fig. 3. The detailed analysis shows that the radius of the interference rings depends strongly on the phase difference. The intensity distribution [calculated from Eq. (7)] is plotted for various values of $\delta_r$, assuming $N = 2$ ($d = 1751.6$ $\mu$m). The values of coefficient $K$ were 0, 0.15, 0.5, and 1.5 for cases depicted in Fig. 4(a), (b), (c), and (d), respectively. As in Fig. 3, the numbers adjacent to the peaks display the value of the peak intensity. The insets in the top-right corner show the intensity immediately in front of the lens. For case (d) it should be noted that a different scale was used because the intensity immediately in front

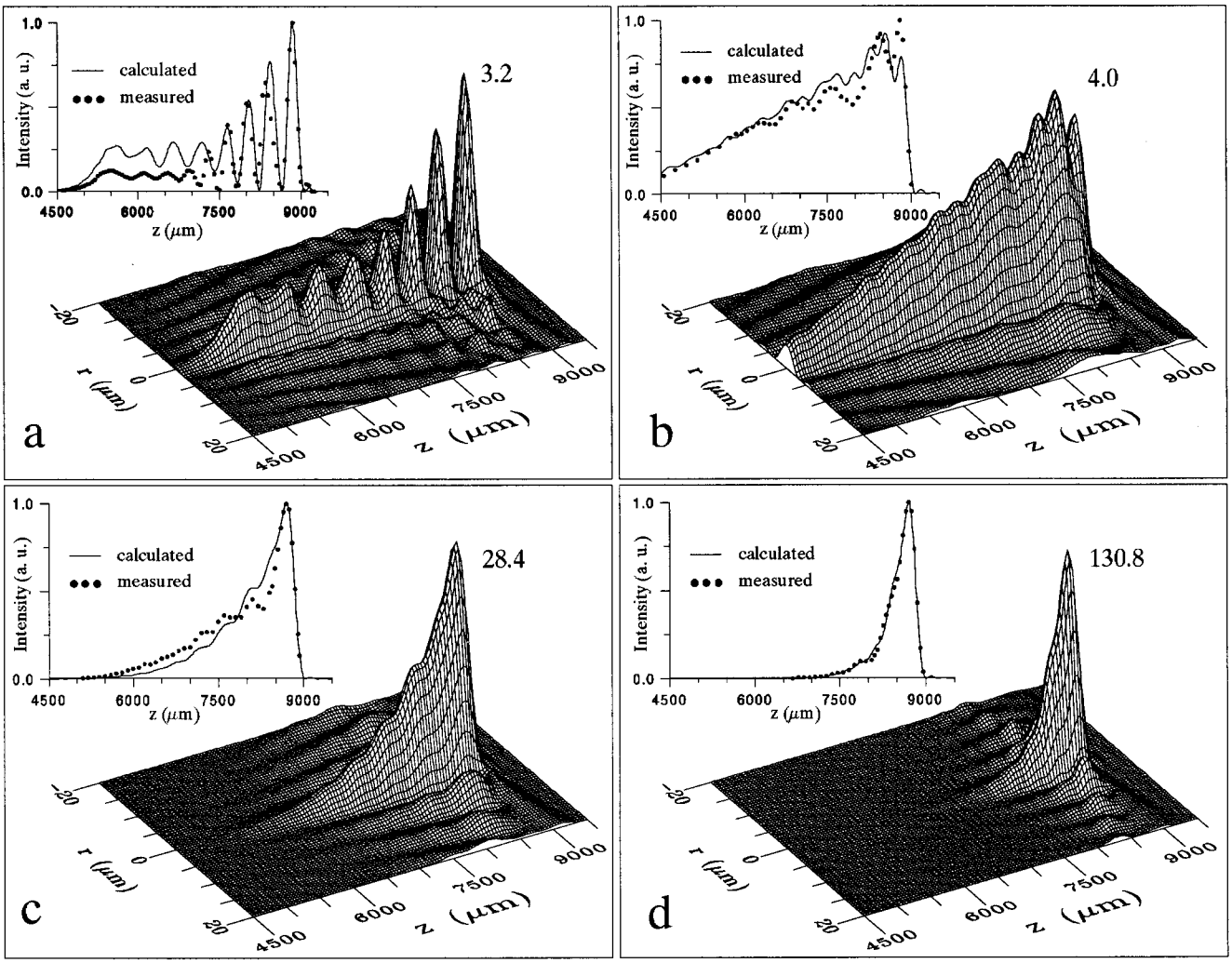


Fig. 3. The spatial intensity distribution as calculated from Eq. (7) for different values of image density $N$ and reduced phase difference $\delta_r$ [see Eqs. (11) and (9)]. The insets show a comparison of the measured and calculated axial intensity distribution. The numbers adjacent to the peaks display the intensity maxima in arbitrary units.

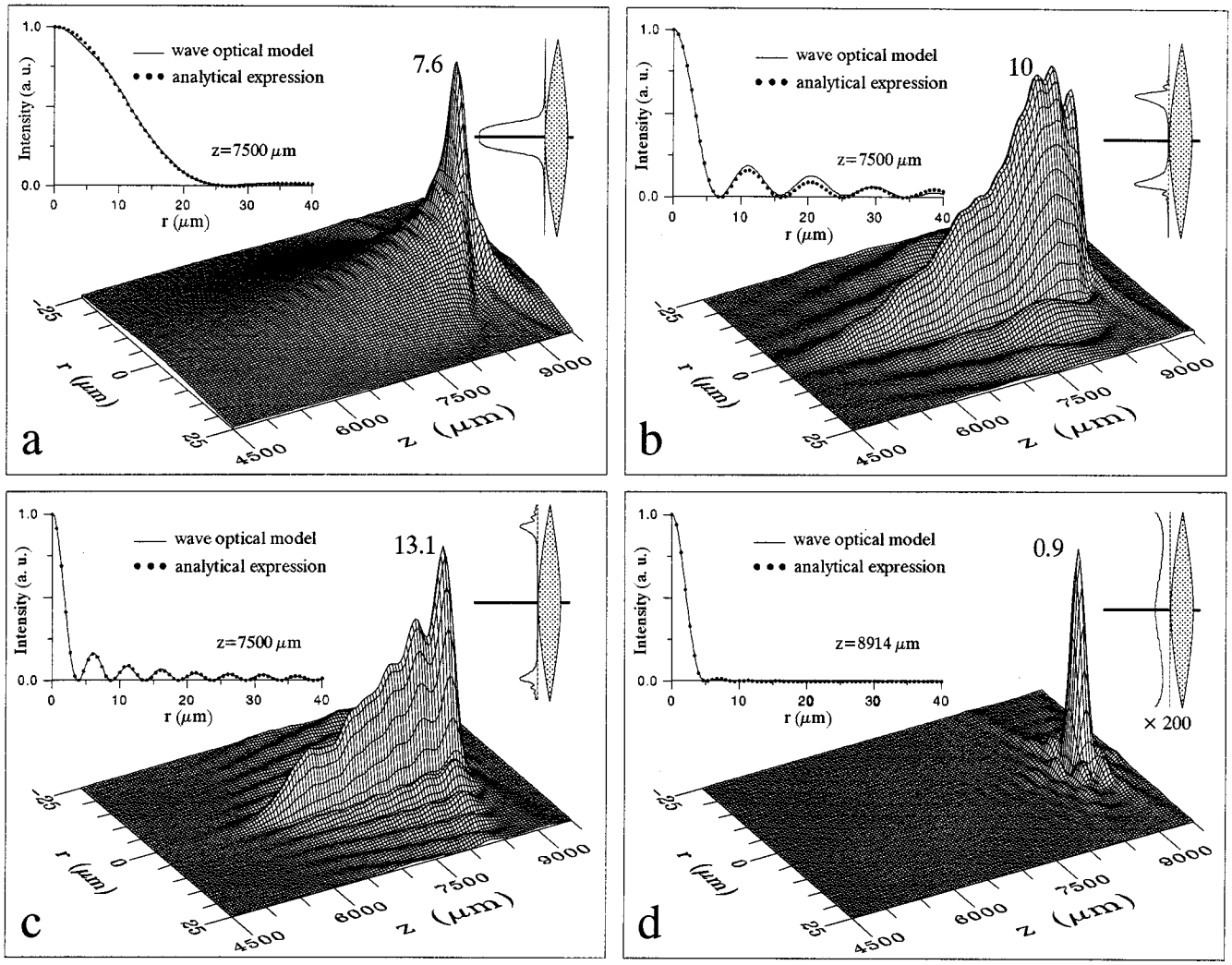


Fig. 4. The spatial intensity distribution, as calculated from Eq. (7), as a function of the reduced phase difference $\delta_r$, assuming approximately constant image density ($N = 2$). The numbers adjacent to the peaks display the intensity maxima in arbitrary units. The insets on the right side show the illumination of the lens. The insets on the left display a comparison of the radial intensity distribution calculated from Eq. (7) and from approximate analytical expressions [Eqs. (12) and (14)]. In case (d) the intensity is decreased considerably, and therefore a different scale was used.

of the lens was much less than that for cases (a)–(c). The electric field in front of the lens can be calculated as the sum of the electric fields produced by point sources $I_0, I_1, \ldots, I_m, \ldots$. The insets in the top-left corner show the radial intensity distribution in a plane perpendicular to $z$. The solid curves indicate the radial intensity distribution calculated from Eq. (7), and the dots display the result of the approximate analytical expressions derived below. In case (a), where $\delta_r = 0$ ($d$ is a multiple of $\lambda/2$), a small, nearly homogeneous bright spot can be seen on the center of the lens, and the first Fabry–Perot ring is beyond the lens aperture. The intensity distribution is like a top-hat profile; thus, the diffraction pattern in a plane perpendicular to $z$ is similar to an Airy-type diffraction pattern given by Ref. 13,

$$I_A(v) = I_{A0}\left(\frac{2J_1(v)}{v}\right)^2, \tag{12}$$

where $I_{A0}$ is the intensity on the axis at a point $z$ and

$$v = \frac{2\pi}{\lambda}\frac{l_A}{f+z}r. \tag{13}$$

In Eq. (13) $l_A$ is the radius of the illuminated area. In Fig. 4(a) the circles show an Airy-type diffraction pattern calculated from Eq. (12) with $l_A = 0.81$ mm. This is the distance at which the amplitude is one half of that on the axis immediately in front of the lens. When $\delta_r$ is increased, the center of the spot becomes dented, and finally a ring is formed. When $\delta_r$ is further increased, the radius of the ring increases and therefore the interference rings shrink in a plane perpendicular to the axis [see Figs. 4(b) and 4(c)]. Then the radial intensity distribution can approximately be described by

$$I_B(r) = I_{B0}J_0{}^2\left(\frac{2\pi}{\lambda}\frac{l_B}{z}r\right), \tag{14}$$

where $I_{B0}$ is the intensity on the axis at point $z$ and

$$l_B = f\sqrt{\left(\frac{K}{2\Lambda} + 1\right)^2 - 1} = f \tan \theta_\Lambda . \qquad (15)$$

Eq. (14) was plotted as dots in Fig. 4(b) and 4(c). The radial intensity distribution can be explained with a simple model. The Fabry–Perot interferometer transmits the light in directions $\theta_m$ given by $\cos \theta_m = m/(2d/\lambda)$, where $m$ is an integer between 1 and $2d/\lambda$. The integral value of $\Lambda$ corresponds to the smallest angle $\theta_\Lambda$. The light incident on the lens in direction $\theta_\Lambda$ is collected by the lens to a bright interference fringe in the focal plane. The radius of the fringe is given by $l_B = f \tan \theta_\Lambda$. Using $\tan^2 \theta_\Lambda = 1/\cos^2 \theta_\Lambda - 1$ and the definition of $K$, one can obtain Eq. (15) for $l_B$. Only one fringe is formed in the focal plane because the lens aperture is adjusted so that it transmits only the first Fabry–Perot ring and blocks all others. At a point $z$ the light arrives from a bright narrow ring lying in the focal plane. The radial intensity distribution of the diffraction pattern of a narrow ring can be described by Eq. (14).

When $\delta_r$ is further increased, the ring moves beyond the lens aperture and the intensity in front of the lens decreases considerably. The illumination of the lens is again homogeneous, and therefore the intensity distribution resembles a three-dimensional Airy pattern [Fig. 4(d)]. The inset on the left side of Fig. 4(d) shows a comparison of the radial intensity distribution calculated from Eq. (7) (solid curve) and from Eq. (12) (dots) with $l_A = a$ in a plane given by $z = 8914\ \mu$m, where the intensity reaches its maximum on the axis.

## 4. CONCLUSION

A new concept for generating nearly nondiffracting Bessel beams has been studied theoretically. The spatial intensity distribution has been calculated with a wave optics model for various values of the image density and phase difference. Approximate analytical expressions have been derived to describe the radial intensity distribution in planes perpendicular to the optical axis.

## ACKNOWLEDGMENTS

This work was supported in part by Texas Instruments, by the National Science Foundation under grants DMI-9202639 and INT-9020541, and by the OTKA Foundation of the Hungarian Academy of Sciences (grants T20910, F020889, and W015239).

The authors may be reached as follows: Z. L. Horváth, e-mail: Z.Horvath@physx.u-szeged.hu. F. K. Tittel can be reached by tel: 713-527-4833 and e-mail: fkt@rice.edu.

## REFERENCES

1. J. Durnin, J. J. Miceli, Jr., and J. H. Eberly, "Diffraction-free beams," Phys. Rev. Lett. **58**, 1499–1501 (1987).
2. R. Arimoto, C. Saloma, T. Tanaka, and S. Kawata, "Imaging properties of axicons in a scanning optical system," Appl. Opt. **31**, 6653–6657 (1992).
3. J. Turunen, A. Vasara, and A. T. Friberg, "Holographic generation of diffraction-free beams," Appl. Opt. **27**, 3959–3962 (1988).
4. A. J. Cox and D. C. Dibble, "Holographic reproduction of a diffraction-free beam," Appl. Opt. **30**, 1330–1332 (1991).
5. A. J. Cox and D. C. Dibble, "Nondiffracting beams from a spatially filtered Fabry–Perot resonator," J. Opt. Soc. Am. A **9**, 282–286 (1992).
6. G. Indebetouw, "Nondiffracting optical fields: some remarks on their analysis and synthesis," J. Opt. Soc. Am. A **6**, 150–152 (1989).
7. J. K. Jabczynski, "A 'diffraction-free' resonator," Opt. Commun. **77**, 292–294 (1990).
8. K. Uehara and H. Kikuchi, "Generation of nearly diffraction-free laser beams," Appl. Phys. B **48**, 125–129 (1989).
9. M. Erdélyi, Z. L. Horváth, G. Szabó, Zs. Bor, F. K. Tittel, J. R. Cavallaro, and M. C. Smayling, "Generation of diffraction-free beams for application in optical microlithography," J. Vac. Sci. Technol. B **15**, 287–292 (1997).
10. G. B. Airy, "On the diffraction of an annular aperture," Philos. Mag. **18**, January 1841.
11. E. H. Linfoot and E. Wolf, "Diffraction images in systems with annular aperture," Proc. Phys. Soc. B **66**, 145–149 (1953).
12. C. A. Taylor and B. J. Thompson, "Attempt to investigate experimentally the intensity distribution near the focus in error-free diffraction patterns of circular and annular apertures," J. Opt. Soc. Am. **48**, 844–850 (1958).
13. M. Born and E. Wolf, "The three-dimensional light distribution near focus," *Principles of Optics*, 6th [corrected] ed. (Pergamon, Oxford, 1989), Chap. 8.8.